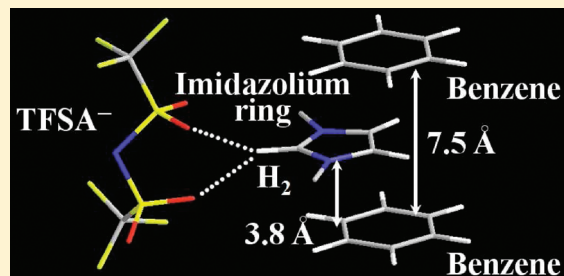


## Clusters of Imidazolium-Based Ionic Liquid in Benzene Solutions

Takuya Shimomura,<sup>†</sup> Toshiyuki Takamuku,<sup>\*,†</sup> and Toshio Yamaguchi<sup>‡</sup><sup>†</sup>Department of Chemistry and Applied Chemistry, Graduate School of Science and Engineering, Saga University, Honjo-machi, Saga 840-8502, Japan<sup>‡</sup>Advanced Materials Institute and Department of Chemistry, Faculty of Science, Fukuoka University, Nanakuma, Jonan-ku, Fukuoka 814-0180, Japan

**ABSTRACT:** Cluster formation of 1-dodecyl-3-methylimidazolium bis(trifluoromethanesulfonyl)amide ( $C_{12}mim^+TFSA^-$ ) in benzene solutions was investigated using small-angle neutron scattering (SANS), NMR, attenuated total reflectance infrared (ATR-IR), and large-angle X-ray scattering (LAXS) techniques. The SANS measurements revealed that  $C_{12}mim^+TFSA^-$  is heterogeneously mixed with benzene in the narrow range of benzene mole fraction  $0.9 \leq x_{C_6D_6} \leq 0.995$  with a maximum heterogeneity at  $x_{C_6D_6} \approx 0.99$ . The NMR results suggested that the imidazolium ring is sandwiched between benzene molecules through the cation– $\pi$  interaction. Moreover,  $TFSA^-$  probably interacts with the imidazolium ring even in the range of  $x_{C_6H_6} \geq 0.9$ . Thus, the imidazolium rings, benzene molecules, and  $TFSA^-$  would form clusters in the  $C_{12}mim^+TFSA^-$ –benzene solutions. The LAXS measurements showed that the distance between the imidazolium ring and benzene is  $\sim 3.8$  Å with that between the benzene molecules of  $\sim 7.5$  Å. On the basis of these results, we discussed a plausible reason for the liquid–liquid equilibrium of the  $C_{12}mim^+TFSA^-$ –benzene system.



## INTRODUCTION

Despite of electrolytes, various imidazolium-based ionic liquids (ILs) with large anions, such as tetrafluoroborate ( $BF_4^-$ ) and hexafluorophosphate ( $PF_6^-$ ), can dissolve in aryl liquids like benzene, toluene, and xylene.<sup>1</sup> Previous investigations on benzene solutions of 1-alkyl-3-methylimidazolium bis(trifluoromethanesulfonyl)amide ( $C_nmim^+TFSA^-$ ,  $n$  represents the number of carbon atoms of the linear alkyl chain) have shown interesting liquid–liquid equilibrium phenomena.<sup>2,3</sup> The phase diagrams of  $C_nmim^+TFSA^-$ –benzene systems revealed that the immiscible (two phase) region is reduced with increasing the alkyl chain length  $n$  of the cations. In the temperature range from 270 to 390 K, the border between miscible (one phase) and immiscible regions of the  $C_4mim^+TFSA^-$ –benzene system is found at a benzene mole fraction of  $x_{C_6H_6} \approx 0.8$ . When  $n = 6$ , an hourglass shape of the immiscible region is observed in the phase diagram. As the alkyl chain length elongates from 8 to 12, the miscibility keeps improving and induces the appearance of the upper critical solution temperature (UCST). The UCSTs are found in the benzene-rich region of  $x_{C_6H_6} > 0.9$ . For instance, the UCST of the  $C_{12}mim^+TFSA^-$ –benzene system is at 281.27 K and  $x_{C_6H_6} = 0.984$ ; the IL is miscible with benzene at any ratio under the ambient conditions (298 K and 0.1 MPa).<sup>3</sup> The lower critical solution temperature (LCST) might be displaced to high temperature out of the range examined ( $> 500$  K). Phase equilibria of 1,3,5-trifluorobenzene and hexafluorobenzene solutions of  $C_2mim^+TFSA^-$  have been compared with that of the benzene system.<sup>5</sup> The phase behaviors of the systems were interpreted by the results of molecular dynamics (MD) simulations. Furthermore, MD simulations have been conducted on the interactions

between  $C_2mim^+TFSA^-$  and 12 fluorinated benzene derivatives, such as 1,4-difluorobenzene and 1,3,5-trifluorobenzene.<sup>6</sup> These simulations indicated that the different quadrupole moments of the aryl molecules may be the key to the phase behaviors. The liquid–liquid equilibria of ILs–aryl liquid systems should be mainly governed by the interactions of cation–aryl molecules and anion–aryl molecules.

The interactions between ILs and aryl molecules have been observed in crystals precipitated from their mixtures using a single-crystal X-ray diffraction technique. In the crystal of  $C_1mim^+PF_6^- \cdot 0.5C_6H_6$ , the cations and anions form a three-dimensional array by hydrogen bonding between the imidazolium hydrogen and fluorine atoms.<sup>1</sup> This leads to the formation of channels along the 001 direction of the crystal. Benzene molecules are individually accommodated into the channels by the interaction between the imidazolium ring and benzene. The X-ray crystallography on  $C_2mim^+TFSA^- \cdot C_6H_6$  has also shown the formation of channels, in which benzene molecules are included.<sup>5</sup> In the crystal, the nearest-neighbor geometry around a benzene molecule has been detailed: three different interactions act on a benzene molecule with two  $C_2mim^+$  and two  $TFSA^-$ . The hydrogen atoms of benzene weakly interact with the  $TFSA^-$  oxygen atoms. The imidazolium hydrogen atom of  $C_2mim^+$  perpendicularly orientates toward the benzene plane due to the  $C-H \cdots \pi$  interaction. Additionally, the other imidazolium ring plane is close to the opposite benzene plane. In the liquid state,

Received: April 12, 2011

Revised: May 30, 2011

Published: May 31, 2011

neutron diffraction measurements have been conducted on 33 and 66 mol % benzene solutions of  $C_{12}\text{mim}^+\text{PF}_6^-$ .<sup>7</sup> The analysis for the diffraction data using an empirical potential structure refinement process showed that the distance between cations in pure IL elongates with increasing benzene content and that benzene molecules exist at both planes of the imidazolium ring, as shown in the crystals. From the other viewpoint, the imidazolium ring occupies positions above and below a benzene plane. Furthermore, benzene molecules interact with the imidazolium hydrogen atoms by the  $\text{C}-\text{H} \cdots \pi$  interaction.

There has been the report on the quantitative analysis on the interaction of the benzene molecule with pyridine, pyridinium, and *N*-methylpyridinium using ab initio calculations with a CCSD(T) level electron correlation correction.<sup>8</sup> Evidently, the benzene–pyridinium and benzene–*N*-methylpyridinium interactions in the slipped-parallel geometry are stronger compared to the benzene–pyridine interaction in the same geometry. This is because both electrostatic and induction interactions greatly contribute to the attraction between the  $\pi$  system of the benzene ring and the positively charged pyridinium. Thus, the former should be categorized into the cation– $\pi$  interaction as opposed to the  $\pi$ – $\pi$  interaction between benzene and neutral pyridine molecules.

Although many investigations have already been reported as above, heterogeneous mixing of ILs with benzene has not been directly observed on a mesoscopic scale. Additionally, the interactions among cation, anion, and benzene molecules in IL–benzene solutions over the entire mole fraction range have not been elucidated on a microscopic scale, except for the neutron diffraction experiments at the two concentrations.<sup>7</sup> Thus, the underlying mechanism of the liquid–liquid equilibria of ILs–benzene solutions has not yet been clarified at the molecular level. In particular, the reason why the immiscible region of ILs–benzene systems is expanded with shortening the alkyl chain of the cation has not been made clear.

In the previous investigation, we have clarified the mixing state of  $C_n\text{mim}^+\text{TFSA}^-$  ( $n = 4$ –12) and protic solvent of methanol by means of small-angle neutron scattering (SANS),  $^1\text{H}$  and  $^{13}\text{C}$  NMR, attenuated total reflectance infrared (ATR-IR) methods.<sup>9</sup> The results suggested that the ILs are heterogeneously mixed with methanol in the methanol mole fraction range of  $0.8 \leq x_{\text{CH}_3\text{OH}} \leq 0.995$ . The weak hydrogen bonds of methanol molecules with the imidazolium ring hydrogen and TFSA<sup>−</sup> oxygen atoms are the important factors of the mixing state of the solutions. Thus, a comparison of the mixing state of the ILs in nonpolar solvent of benzene with that in methanol is of interest.

Here, we report the mixing state of  $C_{12}\text{mim}^+\text{TFSA}^-$ –benzene solutions over the entire benzene mole fraction ( $x_{\text{C}_6\text{H}_6}$ ) range on both mesoscopic and microscopic scales investigated using SANS,  $^1\text{H}$  and  $^{13}\text{C}$  NMR, ATR-IR, and large-angle X-ray scattering (LAXS) techniques.  $C_{12}\text{mim}^+\text{TFSA}^-$ , whose structure is illustrated in Figure 1 with the notation of the hydrogen and carbon atoms, is miscible with benzene at any ratio under the ambient conditions.<sup>3</sup> The heterogeneity of  $C_{12}\text{mim}^+\text{TFSA}^-$ – $\text{C}_6\text{D}_6$  solutions at 298 K were evaluated using a SANS technique. To clarify the interactions of cation–benzene, anion–benzene, and cation–anion,  $^1\text{H}$  and  $^{13}\text{C}$  NMR spectra of the  $C_{12}\text{mim}^+\text{TFSA}^-$ – $\text{C}_6\text{H}_6$  solutions were measured at 298 K. ATR-IR measurements at 298 K were made on the solutions to observe the  $\text{C}-\text{H}$  out-of-plane bending  $\delta_{\text{C}_6\text{H}_6}$  of benzene molecules. Furthermore, LAXS measurements were conducted on  $C_{12}\text{mim}^+\text{TFSA}^-$ – $\text{C}_6\text{H}_6$  solutions at various  $x_{\text{C}_6\text{H}_6}$  to elucidate the structure of

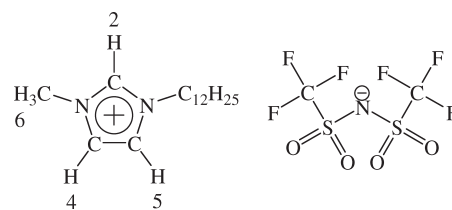


**Figure 1.** Structure of  $C_{12}\text{mim}^+\text{TFSA}^-$  with the position numbers of the hydrogen and carbon atoms.

**Table 1.** Mole Fractions  $x_{\text{C}_6\text{D}_6}$  and Volume Fractions  $\varphi_{\text{C}_6\text{D}_6}$  for the  $C_{12}\text{mim}^+\text{TFSA}^-$ – $\text{C}_6\text{D}_6$  Solutions and the Ornstein–Zernike Correlation Lengths Determined by the SANS Experiments<sup>a</sup>

$x_{\text{C}_6\text{D}_6}$	$\varphi_{\text{C}_6\text{D}_6}$	$\xi/\text{\AA}$
0.800	0.455	
0.900	0.653	3.1(1)
0.950	0.799	10.8(1)
0.970	0.871	22.9(1)
0.980	0.911	39.0(1)
0.990	0.954	50.0(1)
0.995	0.977	31.6(1)

<sup>a</sup> The values in the parentheses are estimated standard deviations of the last figure.

$C_{12}\text{mim}^+\text{TFSA}^-$ –benzene clusters formed in the solutions. Based on the present results, the mixing state of  $C_{12}\text{mim}^+\text{TFSA}^-$ –benzene solutions is discussed on both mesoscopic and microscopic scales. A plausible reason for the alkyl chain length dependence of the miscibility of  $C_n\text{mim}^+\text{TFSA}^-$ –benzene systems is also discussed.

## EXPERIMENTAL SECTION

**Reagents.**  $C_{12}\text{mim}^+\text{TFSA}^-$  was synthesized using the conventional method previously reported.<sup>10</sup> Water content of  $C_{12}\text{mim}^+\text{TFSA}^-$  synthesized was estimated to be less than 50 ppm by a Karl Fischer titration.  $\text{C}_6\text{H}_6$  (Wako Pure Chemicals, grade for HPLC) was adopted for  $^1\text{H}$  and  $^{13}\text{C}$  NMR, ATR-IR, and LAXS experiments. Deuterated benzene,  $\text{C}_6\text{D}_6$ , (Cambridge Isotope Laboratories, D content = 99.8%) was used for SANS experiments to contrast  $\text{C}_6\text{D}_6$  with undeuterated  $C_{12}\text{mim}^+\text{TFSA}^-$  due to the largely different scattering lengths of D and H atoms (+6.67 and −3.74 fm, respectively).

**Sample Solutions.** Sample solutions for SANS experiments were prepared by weighing  $C_{12}\text{mim}^+\text{TFSA}^-$  and  $\text{C}_6\text{D}_6$  at required mole fractions. Mole fractions  $x_{\text{C}_6\text{D}_6}$  and volume fractions  $\varphi_{\text{C}_6\text{D}_6}$  of the sample solutions for SANS experiments are outlined in Table 1.  $C_{12}\text{mim}^+\text{TFSA}^-$ – $\text{C}_6\text{H}_6$  solutions for  $^1\text{H}$  and  $^{13}\text{C}$  NMR, ATR-IR, and LAXS experiments were prepared over the entire  $x_{\text{C}_6\text{H}_6}$  range. Densities of the sample solutions at 298.2 K were measured using an electronic densimeter (Anton Paar GmbH, DSA5000) for analysis of SANS and LAXS data.

**SANS Experiments.** SANS experiments were conducted on the  $C_{12}\text{mim}^+\text{TFSA}^-$ – $\text{C}_6\text{D}_6$  solutions using the SANS-U spectrometer installed at reactor JRR-3 M in the Japan Atomic Energy Agency (JAEA), Tokai, Japan. The sample solutions were kept in a quartz cell of 10 mm in width, 40 mm in height, and 2 mm in sample thickness. The temperature of the solutions was controlled at  $298.2 \pm 0.1$  K. The wavelength of the incident neutron

beam was  $\lambda = 7.0 \text{ \AA}$ , and its size at the sample position was 5 mm in diameter. A two-dimensional position-sensitive detector was placed at camera lengths of 1, 4, and 8 m to cover a wide range of momentum transfer  $q (= 4\pi\lambda^{-1} \sin \theta)$   $6.4 \times 10^{-3}$ – $0.35 \text{ \AA}^{-1}$ .<sup>11,12</sup> The scattering intensities from the sample solution were collected with the detector at the camera lengths of 1, 4, and 8 m for 3, 30, and 60 min, respectively. The observed intensities were corrected for background by subtraction of intensities of an empty cell, and then normalized by dividing the intensities for each sample solution by those for F200-0, a standard low density polyethylene.

**NMR Spectroscopy.**  $^1\text{H}$  and  $^{13}\text{C}$  NMR spectra of the  $\text{C}_{12}\text{mim}^+\text{TFSA}^- - \text{C}_6\text{H}_6$  solutions at 298 K were recorded on an FT-NMR spectrometer (JEOL, JNM-AL300). An external double reference tube (Shigemi), which has a capillary shape with a blown-up sphere at its base, was inserted into the sample tube (Shigemi, PS-001-7). Hexamethyldisiloxane (HMDS) (Wako Pure Chemicals, the first purity grade) was used as a reference substance for  $^1\text{H}$  and  $^{13}\text{C}$  atoms. The observed chemical shifts were corrected for the volume magnetic susceptibility of a sample solution using an external double reference method as described elsewhere.<sup>9,13–16</sup> The digital resolutions of the chemical shift for  $^1\text{H}$  and  $^{13}\text{C}$  NMR measurements were  $\pm 0.0012$  and  $\pm 0.017$  ppm, respectively.

**ATR-IR Spectroscopy.** ATR-IR experiments with a single reflectance were carried out on the  $\text{C}_{12}\text{mim}^+\text{TFSA}^- - \text{C}_6\text{H}_6$  solutions over the entire  $x_{\text{C}_6\text{H}_6}$  range at room temperature using an FT-IR spectrometer (JASCO, FT/IR-6100) equipped with ATR diamond prism (JASCO, PKS-D 470 with ATR PRO450-S). The absorption spectra were accumulated 64 times per sample with a wavenumber resolution of  $4.0 \text{ cm}^{-1}$ . In the ATR-IR spectroscopy, original spectra were corrected for the penetrate depth  $d_p$  of the evanescent wave per reflection by the diamond prism as previously reported.<sup>9</sup>

**LAXS Experiments.** LAXS measurements at 298 K were made on the  $\text{C}_{12}\text{mim}^+\text{TFSA}^- - \text{C}_6\text{H}_6$  solutions at  $x_{\text{C}_6\text{H}_6} = 0, 0.5, 0.8, 0.9, 0.95, 0.97, 0.99, 0.995$ , and 1. A rapid liquid X-ray diffractometer (Bruker AXS, DIP 301) with an imaging plate (IP) (Fuji Film Co.) as a two-dimensional detector was used in the present LAXS experiments. Details of the diffractometer have been described in the literature.<sup>17,18</sup> X-rays were generated at a rotary Mo anode (Rigaku, RU-300) operated at 50 kV and 200 mA and monochromatized by a flat graphite crystal to obtain Mo K $\alpha$  radiation (wavelength  $\lambda = 0.7107 \text{ \AA}$ ). The sample solutions were sealed into a glass capillary (W. Müller Co.) of 2 mm inner diameter with wall thickness of 0.01 mm during measurements. The scattering intensities for the sample solution were accumulated on the IP for 60 min and those for an empty capillary were also measured as background. The observed range of the scattering angle ( $2\theta$ ) was  $0.2^\circ$ – $109^\circ$ , corresponding to the scattering vector  $s (= 4\pi\lambda^{-1} \sin \theta)$  of  $0.03$ – $14.4 \text{ \AA}^{-1}$ .

Two-dimensional X-ray data measured on the IP were first corrected for polarization and integrated to obtain one-dimensional data.<sup>17</sup> The intensities were then corrected for absorption.<sup>18</sup> The intensities of an empty capillary were also measured as background. The contribution of the sample solution alone was obtained by subtracting the intensities for the empty capillary from those for the sample. Finally, the corrected intensities were normalized to absolute units by conventional methods.<sup>19–21</sup> The structure function,  $i(s)$ , for the sample solution was obtained as previously reported<sup>22</sup> and then Fourier transformed into the radial distribution function,  $D(r)$ , in the usual manner.<sup>22</sup> In the

data treatment, the stoichiometric volume  $V$  was chosen to contain one carbon atom in the  $\text{C}_{12}\text{mim}^+\text{TFSA}^- - \text{C}_6\text{H}_6$  solutions. All of the data treatments were made using program KURVLR.<sup>23</sup>

## RESULTS AND DISCUSSION

**SANS Experiments.** Figure 2 shows neutron scattering intensities of the  $\text{C}_{12}\text{mim}^+\text{TFSA}^- - \text{C}_6\text{D}_6$  solutions as a function of  $x_{\text{C}_6\text{D}_6}$ . At  $x_{\text{C}_6\text{D}_6} = 0.8$ , the SANS intensities of the solution are scarcely observed. The SANS intensities of the solutions appear from  $x_{\text{C}_6\text{D}_6} = 0.9$  and are gradually evolved with increasing  $x_{\text{C}_6\text{D}_6}$  to 0.99 where they reach a maximum, followed by a sudden decrease in intensities at  $x_{\text{C}_6\text{D}_6} = 0.995$ . These features show that  $\text{C}_{12}\text{mim}^+\text{TFSA}^-$  is heterogeneously mixed with  $\text{C}_6\text{D}_6$  in the very narrow range of  $0.9 \leq x_{\text{C}_6\text{D}_6} \leq 0.995$ , which corresponds to the volume fraction range of  $0.653 \leq \varphi_{\text{C}_6\text{D}_6} \leq 0.977$ . The heterogeneity of the solutions is most enhanced at  $x_{\text{C}_6\text{D}_6} = 0.99$ .

To quantitatively evaluate the heterogeneity of the  $\text{C}_{12}\text{mim}^+\text{TFSA}^- - \text{C}_6\text{D}_6$  solutions, Ornstein–Zernike fits were performed on the SANS intensities using a least-squares refinement procedure through the equation  $I(q) = I_0/(1 + \xi^2 q^2) + \text{B.G.}$ . Here,  $I_0$  is the scattering intensity at  $q = 0$  and  $\xi$  and B.G. represent the Ornstein–Zernike correlation length and background intensities, respectively. The correlation lengths  $\xi$  determined are listed in Table 1. The theoretical intensities (solid lines in Figure 2) calculated using the  $\xi$  values optimized easily explain the observed ones. In Figure 3, the  $\xi$  values are depicted as a function of  $x_{\text{C}_6\text{D}_6}$  from 0.9 to 0.995. The  $\xi$  value of the solutions at  $x_{\text{C}_6\text{D}_6} = 0.8$  could not be estimated due to scarce SANS intensities. The figure reveals that the heterogeneity of the solution at  $x_{\text{C}_6\text{D}_6} = 0.99$  is higher by a factor of 13 than that at  $x_{\text{C}_6\text{D}_6} = 0.9$ . However, the heterogeneity of the solution at  $x_{\text{C}_6\text{D}_6} = 0.995$  decreases down to 60% of that at  $x_{\text{C}_6\text{D}_6} = 0.99$ . The mole fraction  $x_{\text{C}_6\text{D}_6} = 0.99$  of the maximum heterogeneity of the solutions agrees with the mole fraction of the UCST (276.83 K at  $x_{\text{C}_6\text{D}_6} = 0.9852$ ) of the solutions.<sup>3</sup> Thus, the present SANS experiments might detect IL clusters formed in the solutions as a precursor of phase separation.

The volume fraction range  $0.653 \leq \varphi_{\text{C}_6\text{D}_6} \leq 0.977$  of the heterogeneous mixing of the solutions implies that a smaller amount of  $\text{C}_{12}\text{mim}^+\text{TFSA}^-$  aggregates in a large amount of benzene solvent. However, the Ornstein–Zernike behavior of the SANS intensities of the solutions suggests that the IL clusters do not have a definite shape, such as a micelle, in the solutions. This is the same as  $\text{C}_{12}\text{mim}^+\text{TFSA}^-$ –methanol solutions previously reported.<sup>9</sup> The maximum  $\xi$  (50.0 Å) of the IL–benzene solution at  $x_{\text{C}_6\text{D}_6} = 0.99$  is much larger than that (2.6 Å) of the IL–methanol solution at  $x_{\text{CD}_3\text{OD}} = 0.97$ . This reveals that  $\text{C}_{12}\text{mim}^+\text{TFSA}^-$  clusters are more strongly formed in benzene than in methanol because benzene molecules may not strongly interact with the cation and anion. In contrast, methanol molecules might interact with both ions through the weak hydrogen bonds of  $\text{C}-\text{H} \cdots \text{OH}$  and  $\text{S}=\text{O} \cdots \text{HO}$ .<sup>9</sup>

**$^1\text{H}$  and  $^{13}\text{C}$  NMR Chemical Shifts.** The  $^1\text{H}$  and  $^{13}\text{C}$  NMR chemical shifts of the  $\text{C}_{12}\text{mim}^+\text{TFSA}^- - \text{C}_6\text{H}_6$  solutions with increasing  $x_{\text{C}_6\text{H}_6}$  over the entire range are plotted as a function of  $x_{\text{C}_6\text{H}_6}$  in Figures 4 and 5, respectively. The changes in the chemical shifts of the hydrogen ( $\text{H}_2$ – $\text{H}_6$ ) atoms of  $\text{C}_{12}\text{mim}^+$  with  $x_{\text{C}_6\text{H}_6}$  are comparable with those of the carbon ( $\text{C}_2$ – $\text{C}_6$ ) atoms. All of the atoms are gradually shielded with increasing  $x_{\text{C}_6\text{H}_6}$  to  $\sim 0.9$ . Above  $x_{\text{C}_6\text{H}_6} \approx 0.9$ , the shielding of the  $\text{H}_4$ ,  $\text{C}_4$ ,



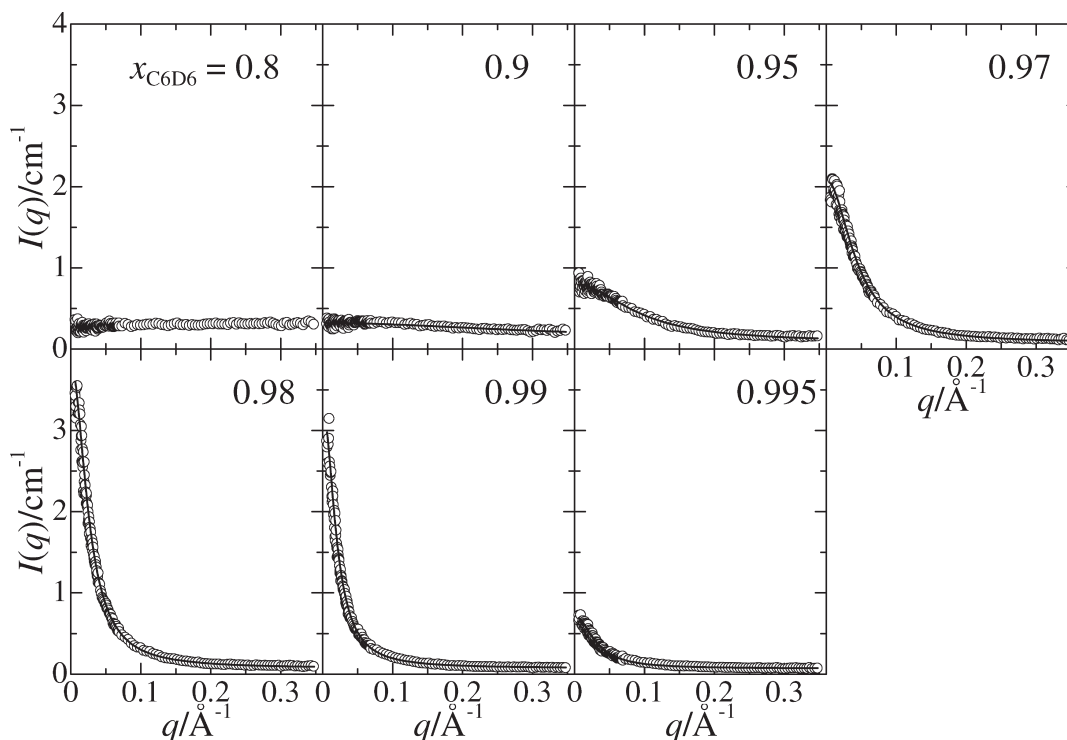


**Figure 2.** SANS intensities of  $\text{C}_{12}\text{mim}^+\text{TFSA}^-$ – $\text{C}_6\text{D}_6$  solutions at various  $x_{\text{C}_6\text{D}_6}$ . The solid lines show the results of least-squares fits using the Ornstein–Zernike equation.

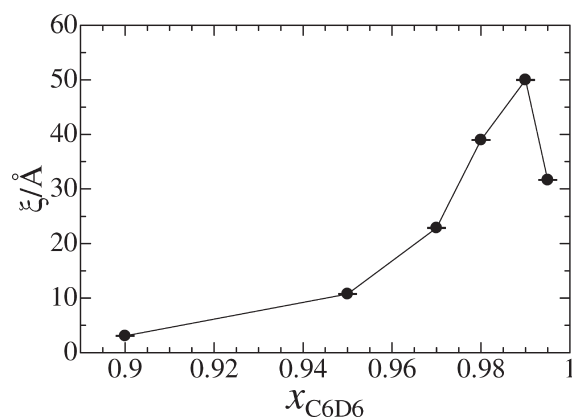


**Figure 3.** Ornstein–Zernike correlation lengths  $\xi$  of  $\text{C}_{12}\text{mim}^+\text{TFSA}^-$ – $\text{C}_6\text{D}_6$  solutions as a function of  $x_{\text{C}_6\text{D}_6}$ .

$\text{H}_5$ , and  $\text{C}_5$  atoms with increasing  $x_{\text{C}_6\text{H}_6}$  becomes more significant. In contrast, the shielding of the  $\text{H}_2$ ,  $\text{C}_2$ ,  $\text{H}_6$ , and  $\text{C}_6$  (the methyl group) becomes moderate above this mole fraction. In both cases, thus, the break points appear at  $x_{\text{C}_6\text{H}_6} \approx 0.9$  in the variations in the chemical shifts.

The interactions among  $\text{C}_{12}\text{mim}^+$ ,  $\text{TFSA}^-$ , and benzene molecules in the  $\text{C}_{12}\text{mim}^+\text{TFSA}^-$ – $\text{C}_6\text{H}_6$  solutions below  $x_{\text{C}_6\text{H}_6} \approx 0.9$  are first considered according to the NMR results. In the previous investigation on  $\text{C}_{12}\text{mim}^+\text{TFSA}^-$ –methanol solutions, the opposite tendency for the NMR data was observed: the imidazolium ring  $\text{H}_2$ – $\text{H}_5$  and  $\text{C}_2$ – $\text{C}_5$  atoms are deshielded with increasing methanol content.<sup>9</sup> The weak  $\text{C}–\text{H} \cdots \text{OH}$  hydrogen bonds between the imidazolium ring hydrogen and methanol contribute to the deshielding of the imidazolium ring

atoms. In contrast, benzene molecules might interact with the imidazolium ring through the cation– $\pi$  interaction. Actually, the spatial distribution functions obtained from the previous MD investigation on the  $\text{C}_2\text{mim}^+\text{TFSA}^-$ –benzene system showed that the  $\text{C}_2$  carbon atom of the imidazolium ring mainly distributes above and below the benzene plane.<sup>4</sup> This is because the quadrupole moment, which lies on the benzene plane, is negative (around  $-30 \times 10^{-40} \text{ C m}^2$ ). Moreover, the ab initio calculations for benzene–pyridinium systems revealed the stronger interaction of the benzene molecule with positively charged pyridinium than neutral pyridine.<sup>8</sup> Thus, the cation– $\pi$  interaction might act between  $\text{C}_{12}\text{mim}^+$  and benzene molecule in the  $\text{C}_{12}\text{mim}^+\text{TFSA}^-$ –benzene solutions. The shielding observed for the  $\text{H}_2$ – $\text{H}_6$  and  $\text{C}_2$ – $\text{C}_6$  atoms of  $\text{C}_{12}\text{mim}^+$  is attributed to the ring current effect of the benzene  $\pi$  electrons because of the parallel geometry between the imidazolium and benzene rings.

The break point at  $x_{\text{C}_6\text{H}_6} \approx 0.9$  in the variations in  $^1\text{H}$  and  $^{13}\text{C}$  NMR chemical shifts of the IL suggests a remarkable change in the mixing state of the solutions. In fact, the point agrees with the SANS results: the formation of IL clusters begins from  $x_{\text{C}_6\text{H}_6} = 0.9$ . Based on the  $^1\text{H}$  and  $^{13}\text{C}$  NMR chemical shifts, the change in the interactions among  $\text{C}_{12}\text{mim}^+$ ,  $\text{TFSA}^-$ , and benzene molecules in the solutions above  $x_{\text{C}_6\text{H}_6} \approx 0.9$  can be interpreted as follows. The moderate shielding of the imidazolium ring  $\text{H}_2$  and  $\text{C}_2$  in the range of  $x_{\text{C}_6\text{H}_6} \geq 0.9$  suggests that the electrostatic interaction between the  $\text{H}_2$  atom and  $\text{TFSA}^-$  is stabilized because of the low dielectric constant of benzene solvent. The previous investigation on the structure of pure  $\text{C}_2\text{mim}^+\text{TFSA}^-$  by LAXS technique and MD simulations showed that the imidazolium ring  $\text{H}_2$ ,  $\text{H}_4$ , and  $\text{H}_5$  atoms interact with the oxygen atoms of the  $-\text{SO}_2(\text{CF}_3)$  groups of  $\text{TFSA}^-$ .<sup>24</sup> In particular, the most positively charged  $\text{H}_2$  atom<sup>25,26</sup> strongly interact with the

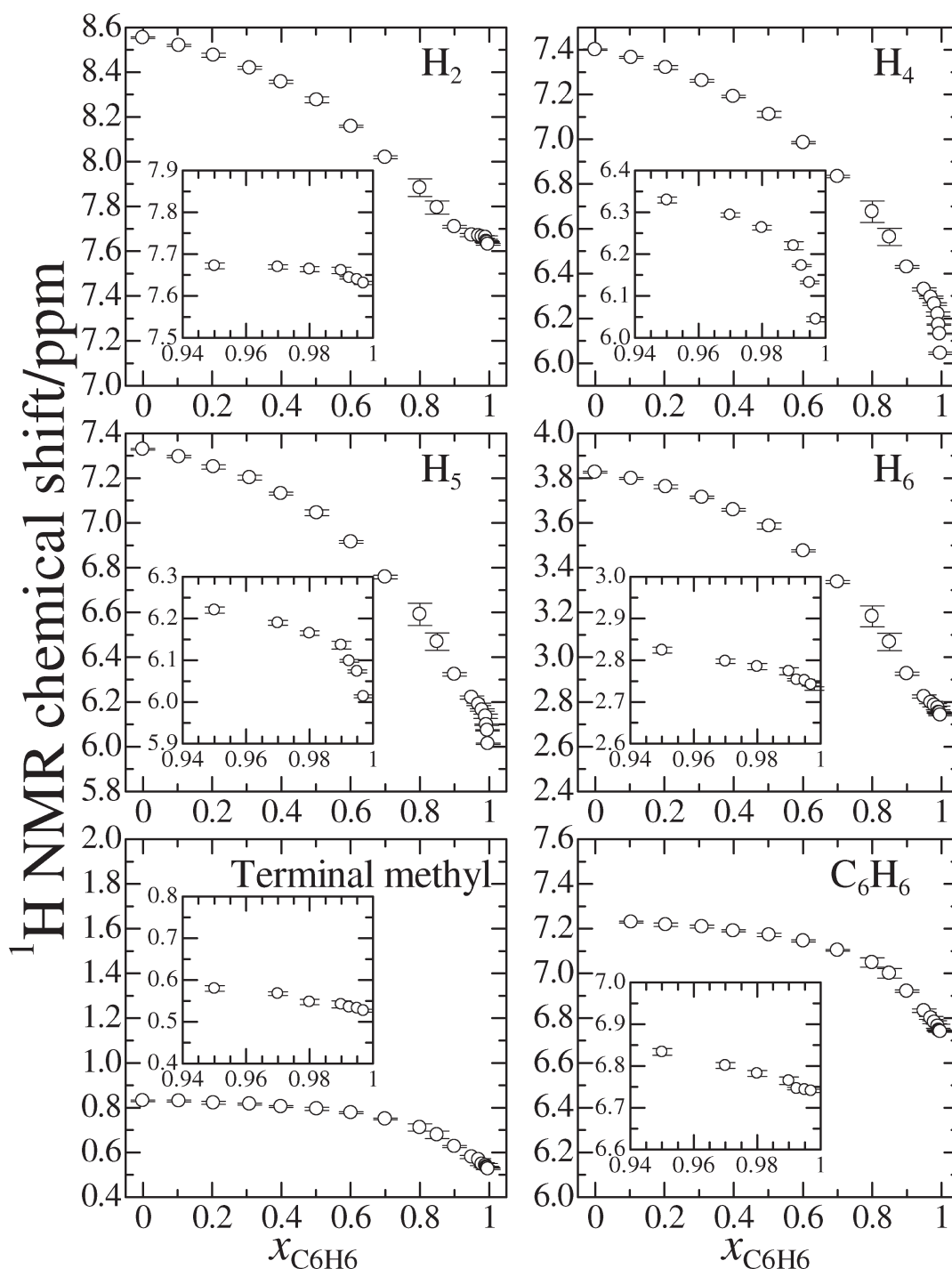


**Figure 4.**  $^1\text{H}$  NMR chemical shifts of  $\text{C}_{12}\text{mim}^+\text{TFSA}^- - \text{C}_6\text{H}_6$  solutions as a function of  $x_{\text{C}_6\text{H}_6}$ . The inset figures show  $^1\text{H}$  NMR chemical shift of each atom expanded in the  $x_{\text{C}_6\text{H}_6}$  range from 0.94 to 1. The estimated standard deviations  $\sigma$  are indicated as error bars.

TFSA<sup>−</sup> oxygen. The attractive force between the H<sub>2</sub> atom and TFSA<sup>−</sup> becomes stronger in the solutions with increasing non-polar benzene content. The change in the  $^{13}\text{C}$  NMR chemical shifts of TFSA<sup>−</sup> is consistent with this consideration. The TFSA<sup>−</sup> carbon atoms are gradually deshielded with increasing  $x_{\text{C}_6\text{H}_6}$ . This is because the electrons of the carbon atoms flow to the oxygen because of the strengthening of the C–H $\cdots$ O=S interaction. The deshielding of the TFSA<sup>−</sup> carbon atoms becomes moderate above  $x_{\text{C}_6\text{H}_6} \approx 0.9$ . This suggests the stable

interaction between the H<sub>2</sub> and the TFSA<sup>−</sup> oxygen above this mole fraction.

Above the break point of  $x_{\text{C}_6\text{H}_6} \approx 0.9$ , the NMR behavior of the H<sub>4</sub>, C<sub>4</sub>, H<sub>5</sub>, and C<sub>5</sub> atoms differs from that of the H<sub>2</sub> and C<sub>2</sub> atoms, as described above. These atoms are more shielded with further increasing benzene content from  $x_{\text{C}_6\text{H}_6} \approx 0.9$ . Particularly, the shielding of the atoms is more conspicuous above  $x_{\text{C}_6\text{H}_6} \approx 0.99$ , resulting in the second break point at this mole fraction. These behaviors would be attributed to the ring current effect of

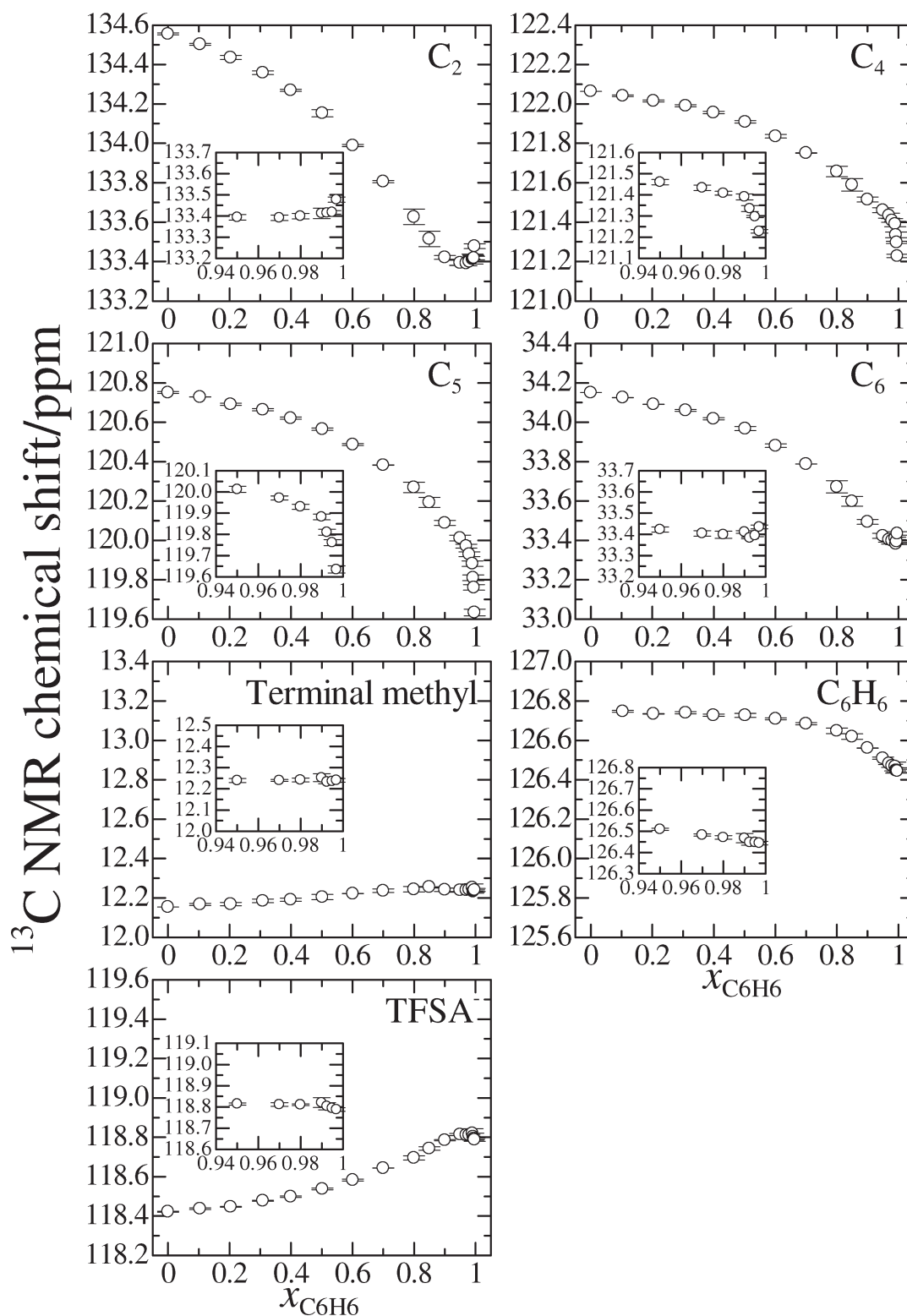


**Figure 5.**  $^{13}\text{C}$  NMR chemical shifts of  $\text{C}_{12}\text{mim}^+\text{TFSA}^- - \text{C}_6\text{H}_6$  solutions as a function of  $x_{\text{C}_6\text{H}_6}$ . The inset figures show  $^{13}\text{C}$  NMR chemical shift of each atom expanded in the  $x_{\text{C}_6\text{H}_6}$  range from 0.94 to 1. The standard deviations  $\sigma$  are indicated as error bars.

the benzene  $\pi$  electrons on the  $\text{H}_4$ ,  $\text{C}_4$ ,  $\text{H}_5$ , and  $\text{C}_5$  atoms. The imidazolium ring  $\text{H}_4$  and  $\text{H}_5$  atoms might interact with the benzene rings through the  $\text{C}-\text{H} \cdots \pi$  interaction. However, the  $\text{H}_4$  and  $\text{H}_5$  atoms interact with the  $\text{TFSA}^-$  oxygen atoms in pure IL.<sup>24</sup> Thus,  $\text{TFSA}^-$  at  $\text{H}_4$  and  $\text{H}_5$  atoms should be replaced by

benzene molecules. The NMR results imply that the replacement significantly occurs above  $x_{\text{C}_6\text{H}_6} \approx 0.99$ . In contrast,  $\text{TFSA}^-$  that interacts with the  $\text{H}_2$  atom is not replaced by a benzene molecule due to the more positively charged  $\text{H}_2$  atom. The present NMR and SANS results suggest that the imidazolium rings, benzene,

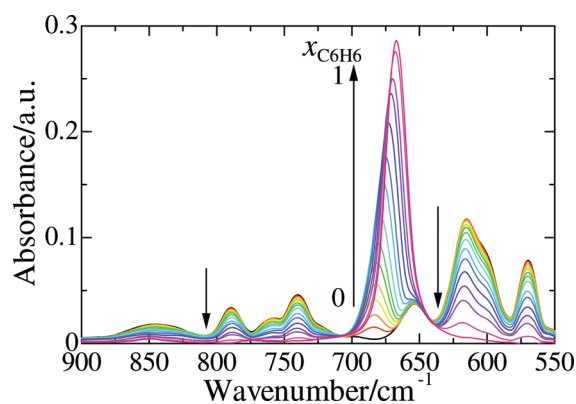


**Figure 6.** ATR-IR spectra of  $C_{12}mim^+TFSA^- - C_6H_6$  solutions at various  $x_{C_6H_6}$ . The arrows indicate the increase in the  $x_{C_6H_6}$ .

and  $TFSA^-$  form IL–benzene clusters through the cation– $\pi$  and C–H $\cdots\pi$  interactions and the electrostatic C–H $\cdots$ O=S interactions in the solutions above  $x_{C_6H_6} \approx 0.9$ . The clusters are most evolved in the solution at  $x_{C_6H_6} \approx 0.99$ .

The deshielding of the terminal methyl carbon of the  $C_{12}mim^+$  alkyl chain is feeble over the entire  $x_{C_6H_6}$  range. The chemical shift of the terminal methyl hydrogen hardly changes with increasing  $x_{C_6H_6}$  to  $\sim 0.8$ . This suggests that the state of the terminal methyl group is not strongly influenced by benzene molecules in the range of  $x_{C_6H_6} \leq 0.8$ . However, the methyl hydrogen atoms are gradually shielded with further increasing  $x_{C_6H_6}$  from  $\sim 0.8$ . It is noteworthy that the hydrogen atoms of hexane are gradually shielded in hexane–benzene solutions when the benzene content increases.<sup>27</sup> This implies that the hydrogen atoms of hexane interact with the  $\pi$  electrons of benzene molecules. In the present NMR results, hence, the shielding of the terminal methyl hydrogen atoms of  $C_{12}mim^+$  above  $x_{C_6H_6} \approx 0.8$  arises from the interaction between the terminal methyl groups and benzene molecules. However, the change in the chemical shift of the terminal methyl hydrogen atoms with increasing  $x_{C_6H_6}$  is smaller compared to that of the imidazolium hydrogen atoms. Thus, benzene molecules less favorably interact with the terminal methyl group compared to the imidazolium ring.

In Figures 4 and 5, the changes in the chemical shifts of the benzene hydrogen and carbon atoms with increasing  $x_{C_6H_6}$  reflect all of the states of benzene molecules in the  $C_{12}mim^+TFSA^- - C_6H_6$  solutions; benzene molecules might interact with the imidazolium plane and its hydrogen atoms and benzene molecules themselves. A break point is observed at  $x_{C_6H_6} \approx 0.8$  in both changes in the  $^1H$  and  $^{13}C$  NMR chemical shifts of benzene. The moderate changes in the NMR values below  $x_{C_6H_6} \approx 0.8$  suggest that benzene molecules are mainly accommodated into the inherent structure of IL through the cation– $\pi$  interaction. In the range of  $x_{C_6H_6} \geq 0.8$ , benzene molecules begin to interact with the imidazolium hydrogen atoms by the C–H $\cdots\pi$  interaction. However, the interactions among a large number of benzene molecules, such as C–H $\cdots\pi$  and  $\pi$ – $\pi$  interactions,<sup>28</sup> more contribute to the conspicuous shielding of both hydrogen and carbon atoms above  $x_{C_6H_6} \approx 0.8$ . Thus, benzene molecules would aggregate with themselves to form clusters in the solutions.

**ATR-IR Spectroscopy.** Figure 6 shows the ATR-IR spectra of the  $C_{12}mim^+TFSA^- - C_6H_6$  solutions in the wavenumber range from 550 to 900  $cm^{-1}$ . In the spectrum of pure benzene ( $x_{C_6H_6} = 1$ ),

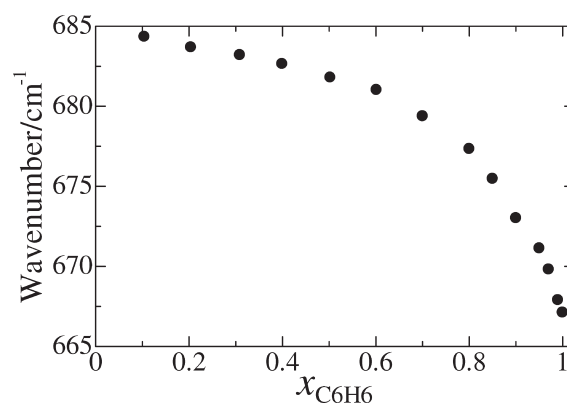


**Figure 7.** Wavenumber for the C–H out-of-plane bending vibration  $\delta_{C_6H_6}$  of benzene as a function of  $x_{C_6H_6}$ .

a prominent peak is observed at 667  $cm^{-1}$ . This peak arises from the C–H out-of-plane bending,  $\delta_{C_6H_6}$ , of the benzene molecule.<sup>29</sup> On the other hand, in the spectrum of pure  $C_{12}mim^+TFSA^-$  ( $x_{C_6H_6} = 0$ ), five peaks are observed at 570, 600, 615, 654, and 740  $cm^{-1}$ . These are assigned to the molecular vibrations of  $TFSA^-$ : the  $CF_3$  asymmetric bending, the  $SO_2$  out-of-plane asymmetric bending, the  $SO_2$  in-plane asymmetric bending, the S–N–S bending, and the  $CF_3$  symmetric bending, respectively.<sup>30,31</sup> Three small peaks above 750  $cm^{-1}$  are attributed to the H–C–C–H asymmetric bending vibrations (758 and 790  $cm^{-1}$ ) and the N–C(H)–N bending vibration (846  $cm^{-1}$ ) of the imidazolium ring, respectively.<sup>31</sup> To discuss the state of benzene molecules in the solutions, we focus on the  $\delta_{C_6H_6}$  band at 667  $cm^{-1}$ .

The C–H out-of-plane bending  $\delta_{C_6H_6}$  band was first fitted by a single pseudo-Voigt function consisting of Lorentzian and Gaussian components to exactly determine the wavenumber of the band. Figure 7 represents the wavenumber of the  $\delta_{C_6H_6}$  band determined as a function of  $x_{C_6H_6}$ . The  $\delta_{C_6H_6}$  band monotonically shifts to the lower frequency with increasing  $x_{C_6H_6}$  to  $\sim 0.8$ . The low frequency shift of the  $\delta_{C_6H_6}$  band becomes more remarkable above  $x_{C_6H_6} \approx 0.8$ . This results in a break point at  $x_{C_6H_6} \approx 0.8$ . The break point agrees with those in the  $^1H$  and  $^{13}C$  NMR data of benzene molecules in the solutions (Figures 4 and 5). The coincidence suggests that the state of benzene molecules in the  $C_{12}mim^+TFSA^- - C_6H_6$  solutions significantly changes at  $x_{C_6H_6} \approx 0.8$ .

Over the entire  $x_{C_6H_6}$  range, the wavenumber of the  $\delta_{C_6H_6}$  band in the solutions is not as low as that of pure benzene. The previous investigation has shown that nonpolar solvents, such as cyclohexane and *n*-heptane, scarcely influence the wavenumber of the  $\delta_{C_6H_6}$  band of benzene, whereas polar solvents, such as acetone and acetonitrile, move the band to the higher frequency.<sup>29</sup> These facts suggest that the interaction between benzene molecule and polar solvents induce the high frequency shift of the  $\delta_{C_6H_6}$  band. In addition, the wavenumber of the  $\delta_{C_6H_6}$  band of crystalline benzene is higher than that of liquid benzene. This is caused by the C–H $\cdots\pi$  interaction between benzene molecules. Hence, the band of the C–H out-of-plane bending shifts to a high frequency, when the benzene hydrogen interacts with the neighbor molecules.<sup>32,33</sup> Thus, benzene molecules in the  $C_{12}mim^+TFSA^- - C_6H_6$  solutions might interact with both IL and benzene themselves. Actually, the previous X-ray diffraction investigation on  $C_2mim^+TFSA^- - C_6H_6$  1:1 inclusion crystal has shown the existence of hydrogen-bond-like

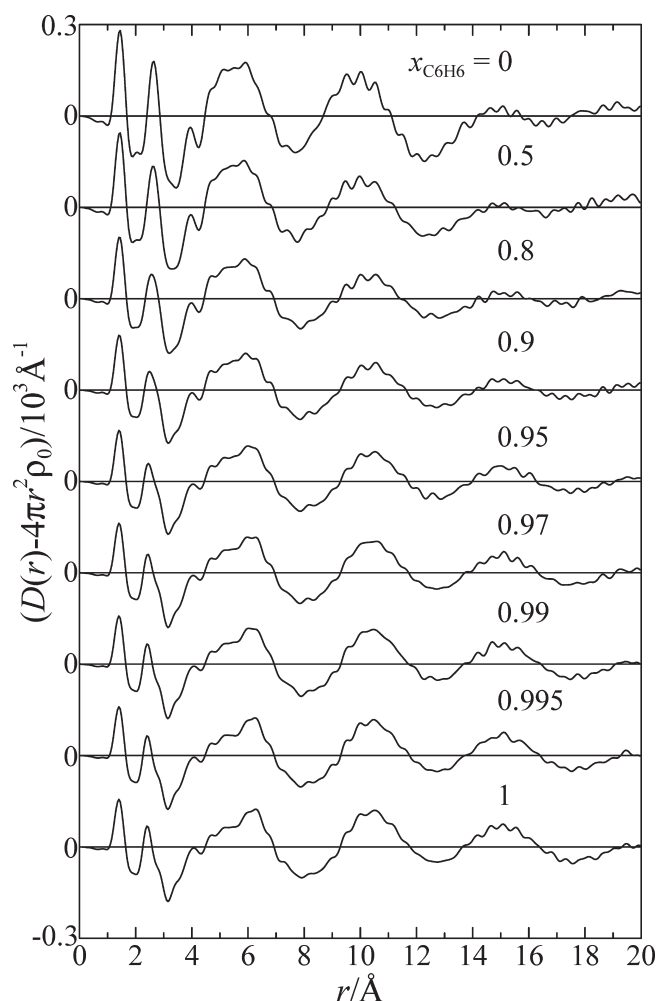


**Figure 8.** RDFs in the form of  $D(r) - 4\pi r^2 \rho_0$  for  $C_{12}mim^+TFSA^- - C_6H_6$  solutions at various  $x_{C_6H_6}$ .

interactions between the benzene hydrogen and the  $TFSA^-$  oxygen atoms.<sup>5</sup> A similar interaction is shown in the solvation structure of  $C_2mim^+TFSA^-$ –benzene solutions.<sup>4</sup> Consequently, benzene molecules interact with  $TFSA^-$  and the imidazolium ring hydrogen in the solutions below  $x_{C_6H_6} \approx 0.8$ . However, the inherent structure of benzene is evolved in the solutions above  $x_{C_6H_6} \approx 0.8$ , resulting in the drastic shift to the value of pure benzene.

**LAXS Experiments.** Figure 8 shows the radial distribution functions (RDFs) in the form of  $D(r) - 4\pi r^2 \rho_0$  for the  $C_{12}mim^+TFSA^- - C_6H_6$  solutions obtained from the LAXS experiments. As previously reported,<sup>24</sup> two sharp peaks at 1.4 and 2.6 Å in the RDF for pure  $C_{12}mim^+TFSA^-$  ( $x_{C_6H_6} = 0$ ) are ascribed to the intramolecular interactions within  $C_{12}mim^+$  and  $TFSA^-$ ; the first peak is mainly assigned to the C–C, C–N, C–F, N–S, and S=O bonds, and the second peak arises from the nonbonding interactions of  $C \cdots C$ ,  $C \cdots N$ , and  $S \cdots S$ . Two broad peaks centered at  $\sim 5.6$  and  $\sim 10$  Å are mainly attributed to the first neighbor  $C_{12}mim^+ \cdots TFSA^-$  interactions and the second neighbor  $C_{12}mim^+ \cdots C_{12}mim^+$  and  $TFSA^- \cdots TFSA^-$  interactions, respectively. The  $TFSA^- \cdots TFSA^-$  interactions more significantly contribute to the peak at  $\sim 10$  Å than the  $C_{12}mim^+ \cdots C_{12}mim^+$  interactions due to the large X-ray scattering factors of F and S atoms. In the RDF for benzene

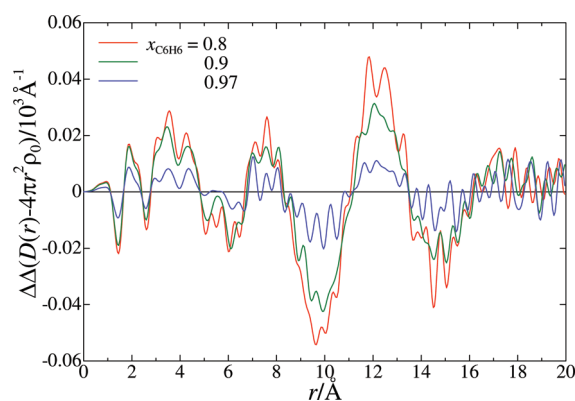


**Figure 9.** Double differential RDFs for  $C_{12}mim^+TFSA^- - C_6H_6$  solutions obtained by subtracting the composite of the concentration weighed RDFs for neat  $C_{12}mim^+TFSA^-$  and  $C_6H_6$  from the original RDFs for  $C_{12}mim^+TFSA^- - C_6H_6$  solutions.

( $x_{C_6H_6} = 1$ ), two peaks at 1.4 and 2.5 Å arise from the C–C and  $C \cdots C$  interactions within benzene molecule. The first neighbor interactions among benzene molecules are observed at  $\sim 5.7$  Å, and the second neighbor ones are shown at  $\sim 11$  Å. A peak at  $\sim 15$  Å shows the long-range ordering in pure benzene. In the RDFs for the  $C_{12}mim^+TFSA^- - C_6H_6$  solutions, the peak at 10 Å in the RDF for  $C_{12}mim^+TFSA^-$  gradually shifts to the longer-range with increasing  $x_{C_6H_6}$ . The valley at  $\sim 12$  Å in the RDF for the IL becomes shallower with increasing  $x_{C_6H_6}$  to 0.8. The third neighbor interactions at 15 Å in benzene begin to appear in the RDF of the solution at  $x_{C_6H_6} = 0.9$ . The RDFs for the solutions at  $x_{C_6H_6} = 0.5$  and 0.8 bear resemblance with that for pure IL. In contrast, the RDFs for the solutions above  $x_{C_6H_6} = 0.9$  are comparable with that for benzene. Thus, the structural change from  $C_{12}mim^+TFSA^-$  to benzene remarkably takes place at  $x_{C_6H_6} \approx 0.8$ .

To clarify the change in the structure of the  $C_{12}mim^+TFSA^- - C_6H_6$  solutions with increasing  $x_{C_6H_6}$ , double differential RDFs (DDRDFs) for the solutions were obtained by subtracting the composite of the concentration weighed RDFs for neat  $C_{12}mim^+TFSA^-$  and  $C_6H_6$  from the original RDFs for the  $C_{12}mim^+TFSA^- - C_6H_6$  solutions at  $x_{C_6H_6} = 0.8, 0.9$ , and 0.97 (Figure 9). Here, the positive peaks observed in the DDRDFs mainly show the cross-term interactions between IL and benzene generated in the solutions by mixing both liquids, whereas the negative ones indicate disruption of the inherent structure of IL and benzene. Two positive peaks appear at  $\sim 3.8$  and  $\sim 7.5$  Å in the DDRDFs and should be due to the interactions between  $C_{12}mim^+TFSA^-$  and  $C_6H_6$ . As discussed on the NMR data, together with the previous investigations by X-ray crystallography,<sup>5</sup> neutron diffraction,<sup>7</sup> and MD simulations,<sup>4,6</sup> the imidazolium ring is sandwiched between benzene molecules. Thus, the peaks at  $\sim 3.8$  and  $\sim 7.5$  Å would be ascribed to the cation– $\pi$  interaction between the  $C_{12}mim^+$  imidazolium ring and the  $\pi$  electrons of benzene molecules. In fact, the van der Waals thickness of the aromatic ring is  $\sim 3.4$  Å. Additionally, the partial distribution function of  $C_2mim^+ \cdots$  benzene interactions obtained by the neutron diffraction<sup>7</sup> showed that the interactions fall in the range from 3.8 to 6 Å. Thus, the first peak centered at  $\sim 3.8$  Å would arise from the interaction between the imidazolium and benzene rings, whereas the second peak at  $\sim 7.5$  Å from the distance between the benzene rings, where the imidazolium ring is inserted.



The large negative peak is observed at  $\sim 10$  Å in the DDRDFs, whereas the large positive peak appears at  $\sim 12$  Å. The large peak at  $\sim 10$  Å in the original RDF for the IL (Figure 8,  $x_{\text{C}_6\text{H}_6} = 0$ ) is mainly ascribed to the  $\text{TFSA}^- \cdots \text{TFSA}^-$  interactions,<sup>24</sup> as described above. Hence, the negative peak at  $\sim 10$  Å in the DDRDF (Figure 9) might be ascribed to a decrease in the  $\text{TFSA}^- \cdots \text{TFSA}^-$  interactions on addition of benzene to the IL. In each DDRDF, the intensity of the large peak at  $\sim 12$  Å might compensate for the height of the negative peak at  $\sim 10$  Å. Thus, the peak at  $\sim 12$  Å could be interpreted as a shift of the  $\text{TFSA}^- \cdots \text{TFSA}^-$  interactions to the longer-range. As discussed above, the distance of the  $\text{C}_{12}\text{mim}^+ \cdots \text{C}_{12}\text{mim}^+$  interactions observed in the IL is elongated by adding benzene because a benzene molecule is intercalated between the imidazolium rings through the cation- $\pi$  interaction. Moreover, the NMR results suggested that the interaction between the imidazolium ring  $\text{H}_2$  atom and  $\text{TFSA}^-$  is not significantly perturbed in the solutions in the range of  $x_{\text{C}_6\text{H}_6} \leq 0.99$ . Thus, the distance of the  $\text{TFSA}^- \cdots \text{TFSA}^-$  interactions should be lengthened on adding benzene. The results from all the present experiments suggest that the  $\text{C}_{12}\text{mim}^+$  imidazolium rings, benzene molecules, and  $\text{TFSA}^-$  may form clusters in the  $\text{C}_{12}\text{mim}^+\text{TFSA}^-$ -benzene solutions.

#### Mixing State of the $\text{C}_{12}\text{mim}^+\text{TFSA}^-$ -Benzene Solutions.

In pure  $\text{C}_{12}\text{mim}^+\text{TFSA}^-$ , the positively charged imidazolium rings and  $\text{TFSA}^-$  might aggregate with themselves to form the polar domains, whereas the dodecyl groups interact with each other to form the nonpolar domains, as shown by the previous MD simulations.<sup>34</sup> When benzene molecules are added into the IL, they are probably first intercalated between the imidazolium rings by the cation- $\pi$  interaction in the polar domains. The present NMR data suggested that the presence of the cation- $\pi$  interaction between the imidazolium ring and benzene is evidence of the shielding of the imidazolium ring  $\text{H}_2$ - $\text{H}_5$  and  $\text{C}_2$ - $\text{C}_5$  atoms due to the ring current effect of benzene molecules intercalated. The X-ray RDFs for the  $\text{C}_{12}\text{mim}^+\text{TFSA}^-$ -benzene solutions at  $x_{\text{C}_6\text{H}_6} = 0.5$  and  $0.8$  are comparable with that of pure IL, showing that the inherent structure of the IL mostly remains in the solutions below  $x_{\text{C}_6\text{H}_6} \approx 0.8$ . Furthermore, the break point at  $x_{\text{C}_6\text{H}_6} \approx 0.8$  observed in the  $^1\text{H}$  and  $^{13}\text{C}$  NMR and ATR-IR data suggests that the state of benzene molecules does not remarkably change in the solutions in the range of  $x_{\text{C}_6\text{H}_6} \leq \sim 0.8$ . In this situation, the concentration fluctuations of the  $\text{C}_{12}\text{mim}^+\text{TFSA}^-$ -benzene solutions would not be generated in the solutions. Thus, the SANS intensities of the solutions were scarcely observed. The present results imply that precursors of liquid clathrates of aryl liquid-IL, where aryl molecules are accommodated in the channels of the inherent IL structure,<sup>1,5</sup> are formed in the IL-aryl liquid solutions. The cation- $\pi$  and  $\text{C}-\text{H} \cdots \pi$  interactions between the imidazolium ring and aryl molecule may play the most important role to form liquid clathrates, as well as liquid clathrates of aryl liquid-complex salt systems with higher melting points, such as  $\text{K}[\text{Al}_2(\text{CH}_3)_6\text{N}_3]$ , than ILs.<sup>35</sup> The ratio of aryl molecule to IL or salt in the liquid clathrates should depend on both sizes of aryl molecules and the channels formed by cations and anions.

The NMR data suggested a strong interaction between the imidazolium ring  $\text{H}_2$  and  $\text{C}_2$  and  $\text{TFSA}^-$  in the solutions. The  $\delta_{\text{C}_6\text{H}_6}$  band of benzene molecules observed by the ATR-IR spectroscopy implied that benzene molecules also interact with  $\text{TFSA}^-$ . Hence, the imidazolium rings, benzene molecules, and  $\text{TFSA}^-$  form the IL-benzene clusters in the polar domains in the  $\text{C}_{12}\text{mim}^+\text{TFSA}^-$ -benzene solutions. In the clusters, the

imidazolium ring bound to  $\text{TFSA}^-$  is probably sandwiched between benzene molecules through the cation- $\pi$  interaction. The X-ray DDRDFs suggested that the distance between the imidazolium ring and benzene molecules is  $\sim 3.8$  Å, whereas that between the benzene molecules intercalating the imidazolium ring is  $\sim 7.5$  Å. It is probable that several units of the imidazolium ring with  $\text{TFSA}^-$  and benzene molecules are stacked in the polar domains of the IL. Furthermore, benzene molecules might interact with the imidazolium  $\text{H}_4$  and  $\text{H}_5$  atoms by the  $\text{C}-\text{H} \cdots \pi$  interaction in the solutions above  $x_{\text{C}_6\text{H}_6} \approx 0.8$ .

In the range of  $x_{\text{C}_6\text{H}_6} > \sim 0.8$ , benzene molecules might also interact with themselves through the  $\text{C}-\text{H} \cdots \pi$  and  $\pi-\pi$  interactions to form benzene clusters in the solutions, as suggested by the NMR and ATR-IR data. In practice, the X-ray RDFs for the  $\text{C}_{12}\text{mim}^+\text{TFSA}^-$ -benzene solutions above  $x_{\text{C}_6\text{H}_6} = 0.9$  are comparable with that of benzene. It is most likely that the benzene clusters are formed around the nonpolar domains of the dodecyl groups grown out from the IL-benzene clusters. This is because the interactions between the imidazolium ring and benzene molecules through the cation- $\pi$  and  $\text{C}-\text{H} \cdots \pi$  interactions are saturated above the ratio of the imidazolium ring to benzene of 1:4, which corresponds to  $x_{\text{C}_6\text{H}_6} = 0.8$ . Moreover, the interaction between the dodecyl groups and benzene molecules would not be so strong as shown in the NMR data. Hence, the IL-benzene clusters of the polar domain, the benzene clusters, and the nonpolar domains of the dodecyl groups would be simultaneously formed in the solutions. In this situation, the concentration fluctuations among the three domains, particularly between benzene clusters and the nonpolar domains, would be generated in the solutions. Consequently, the significant SANS intensities were observed for the solutions above  $x_{\text{C}_6\text{H}_6} = 0.9$ . Both IL-benzene clusters and benzene clusters are most enhanced in the solution at  $x_{\text{C}_6\text{H}_6} \approx 0.99$ , resulting in the maximum  $\xi$  value at the mole fraction. However, the SANS intensities of the solutions were decreased at  $x_{\text{C}_6\text{H}_6} = 0.995$ , implying a decrease in the size of IL-benzene clusters in the solutions above  $x_{\text{C}_6\text{H}_6} \approx 0.99$ . As seen in Figures 4 and 5, the NMR data of the  $\text{H}_4$ ,  $\text{C}_4$ ,  $\text{H}_5$ , and  $\text{C}_5$  atoms of  $\text{C}_{12}\text{mim}^+$  above the second break point  $x_{\text{C}_6\text{H}_6} \approx 0.99$  suggested that the  $\text{H}_4$  and  $\text{H}_5$  atoms of the imidazolium rings are strongly solvated by benzene molecules through the  $\text{C}-\text{H} \cdots \pi$  interaction in the solutions due to a large amount of benzene. This would lead to the loosening of the IL-benzene clusters. While the  $\text{H}_2$  and  $\text{C}_2$  atoms were gradually shielded with increasing  $x_{\text{C}_6\text{H}_6}$  to  $0.99$ , the atoms were deshielded above  $x_{\text{C}_6\text{H}_6} \approx 0.99$ . This deshielding of the  $\text{H}_2$  and  $\text{C}_2$  atoms above  $x_{\text{C}_6\text{H}_6} \approx 0.99$  implies that the interaction between the  $\text{H}_2$  atom of  $\text{C}_{12}\text{mim}^+$  and the oxygen atoms of  $\text{TFSA}^-$  in the solutions is strengthened in the low dielectric constant of benzene, despite of the strong solvation of the  $\text{H}_4$  and  $\text{H}_5$  atoms by benzene molecules. Thus,  $\text{C}_{12}\text{mim}^+$  and  $\text{TFSA}^-$  would form an ion pair in the solutions above  $x_{\text{C}_6\text{H}_6} \approx 0.99$ .

Finally, the liquid-liquid equilibrium behavior of the  $\text{C}_n\text{mim}^+\text{TFSA}^-$ -benzene systems is discussed according to the present results. In the phase diagrams, the immiscible (two phase) region of the binary systems widens to the low  $x_{\text{C}_6\text{H}_6}$  range with shortening the alkyl chain of  $\text{C}_n\text{mim}^+$ .<sup>2,3</sup> The previous MD simulations showed that the microphase separation between the polar domains consisting of the imidazolium rings and anions and the nonpolar domains of the alkyl chains occurs in pure  $\text{C}_n\text{mim}^+\text{TFSA}^-$  with the alkyl chain length  $n = 4-12$ .<sup>34</sup> The shorter the alkyl chain, the smaller the nonpolar domains are formed in the ILs. When benzene is added into the ILs, probably,

the formation of the IL–benzene clusters in the polar domains does not significantly depend on the alkyl chain length. This is probably because the interactions of cation– $\pi$ , C–H $\cdots\pi$ , and the electric force between  $C_n\text{mim}^+$  and  $\text{TFSA}^-$  are not different among the ILs. Thus, the IL–benzene clusters of the polar domains are gradually formed in all IL–benzene solutions with increasing benzene content in a similar manner. When the interactions among the imidazolium rings, benzene molecules, and  $\text{TFSA}^-$  in the polar domains are saturated, benzene molecules would begin to form the benzene clusters around the nonpolar domains of the alkyl groups. The repulsive force may act between the benzene clusters and the IL–benzene clusters of the polar domains. The force will become stronger with shortening the alkyl chain because both clusters are close to each other due to the smaller nonpolar domains of the alkyl chains as a cushioning. This is a plausible reason for the alkyl chain length dependence of the liquid–liquid equilibrium behavior of  $C_n\text{mim}^+\text{TFSA}^-$ –benzene systems.

## AUTHOR INFORMATION

### Corresponding Author

\*E-mail: takamut@cc.saga-u.ac.jp.

## ACKNOWLEDGMENT

This work was supported partly by Grants-in-Aid (No. 22550018 and 23103704) from the Japan Society for the Promotion of Science and by Saga University Dean's Grant 2010 for Promising Excellent Research Projects. The SANS experiments were carried out under the Joint-use Research Program for Neutron Scattering, Institute for Solid State Physics (ISSP), the University of Tokyo, at the Research Reactor JRR-3M, JAEA (Proposal No.8851 and 9603). The density and NMR measurements for the sample solutions were conducted at the Analytical Research Center for Experimental Sciences of Saga University.

## REFERENCES

- (1) Holbrey, J. D.; Reichert, W. M.; Nieuwenhuyzen, M.; Sheppard, O.; Hardacre, C.; Rogers, R. D. *Chem. Commun.* **2003**, 476.
- (2) Łachwa, J.; Szydłowski, J.; Makowska, A.; Seddon, K. R.; Esperança, J. M. S. S.; Guedes, H. J. R.; Rebelo, L. P. N. *Green Chem.* **2006**, 8, 262.
- (3) Makowska, A.; Siporska, A.; Szydłowski, J. *Fluid Phase Equilib.* **2009**, 282, 108.
- (4) Blesic, M.; Lopes, J. N. C.; Pádua, A. A. H.; Shimizu, K.; Gomes, M. F. C.; Rebelo, L. P. N. *J. Phys. Chem. B* **2009**, 113, 7631.
- (5) Łachwa, J.; Bento, I.; Duarte, M. T.; Lopes, J. N. C.; Rebelo, L. P. N. *Chem. Commun.* **2006**, 2445.
- (6) Shimizu, K.; Gomes, M. F. C.; Pádua, A. A. H.; Rebelo, L. P. N.; Lopes, J. N. C. *J. Phys. Chem. B* **2009**, 113, 9894.
- (7) Deetlefs, M.; Hardacre, C.; Nieuwenhuyzen, M.; Sheppard, O.; Soper, A. K. *J. Phys. Chem. B* **2005**, 109, 1593.
- (8) Tsuzuki, S.; Mikami, M.; Yamada, S. *J. Am. Chem. Soc.* **2007**, 129, 8656.
- (9) Shimomura, T.; Fujii, K.; Takamuku, T. *Phys. Chem. Chem. Phys.* **2010**, 12, 12316.
- (10) Nockemann, P.; Binnemans, K.; Driesen, K. *Chem. Phys. Lett.* **2005**, 415, 131.
- (11) Okabe, S.; Nagao, M.; Karino, T.; Watanabe, S.; Adachi, T.; Shimizu, H.; Shibayama, M. *J. Appl. Crystallogr.* **2005**, 38, 1035.
- (12) Okabe, S.; Karino, T.; Nagao, M.; Watanabe, S.; Shibayama, M. *Nucl. Inst. Meth. A* **2007**, 572, 853.
- (13) Mizuno, K.; Tamiya, Y.; Mekata, M. *Pure Appl. Chem.* **2004**, 76, 105.
- (14) Mizuno, K.; Imafuji, S.; Ochi, T.; Ohta, T.; Maeda, S. *J. Phys. Chem. B* **2000**, 104, 11001.
- (15) Momoki, K.; Fukazawa, Y. *Anal. Chem.* **1990**, 62, 1665.
- (16) Momoki, K.; Fukazawa, Y. *Anal. Sci.* **1994**, 10, 53.
- (17) Yamanaka, K.; Yamaguchi, T.; Wakita, H. *J. Chem. Phys.* **1994**, 101, 9830.
- (18) Ihara, M.; Yamaguchi, T.; Wakita, H.; Matsumoto, T. *Adv. X-ray Anal. Jpn.* **1994**, 25, 49. Yamaguchi, T.; Wakita, H.; Yamanaka, K. *Fukuoka Univ. Sci. Rep.* **1999**, 29, 127.
- (19) Furukawa, K. *Rep. Prog. Phys.* **1962**, 25, 395.
- (20) Krogh-Moe, J. *Acta Crystallogr.* **1956**, 2, 951.
- (21) Norman, N. *Acta Crystallogr.* **1957**, 10, 370.
- (22) Takamuku, T.; Tabata, M.; Yamaguchi, A.; Nishimoto, J.; Kumamoto, M.; Wakita, H.; Yamaguchi, T. *J. Phys. Chem. B* **1998**, 102, 8880.
- (23) Johanson, G.; Sandström, M. *Chem. Scr.* **1973**, 4, 195.
- (24) Fujii, K.; Soejima, Y.; Kyoshoin, Y.; Fukuda, S.; Kanzaki, R.; Umebayashi, Y.; Yamaguchi, T.; Ishiguro, S.; Takamuku, T. *J. Phys. Chem. B* **2008**, 112, 4329.
- (25) Elaiwi, A.; Hitchcock, P. B.; Seddon, K. R.; Srinivasan, N.; Tan, Y.-M.; Welton, T.; Zora, J. A. *J. Chem. Soc., Dalton Trans.* **1995**, 3467.
- (26) Hardacre, C.; Holbrey, J. D.; McMath, S. E. J.; Bowron, D. T.; Soper, A. K. *J. Chem. Phys.* **2003**, 118, 273.
- (27) Kasahara, Y.; Suzuki, Y.; Kabasawa, A.; Minami, H.; Matsuzawa, H.; Iwahashi, M. *J. Oleo Sci.* **2010**, 59, 21.
- (28) Narten, A. H. *J. Chem. Phys.* **1968**, 48, 1630.
- (29) Cole, A. R. H.; Michell, A. J. *Spectrochim. Acta* **1964**, 20, 747.
- (30) Rey, I.; Johansson, P.; Lindgren, J.; Lassègues, J. C.; Grondin, J.; Servant, L. *J. Phys. Chem. A* **1998**, 102, 3249.
- (31) Kiefer, J.; Fries, J.; Leipertz, A. *Appl. Spectrosc.* **2007**, 61, 1306.
- (32) Marzocchi, M. P.; Bonadeo, H. *Chem. Phys. Lett.* **1972**, 14, 282.
- (33) Yamada, H.; Saheki, M. *Bull. Chem. Soc. Jpn.* **1983**, 56, 35.
- (34) Lopes, J. N. A. C.; Pádua, A. A. H. *J. Phys. Chem. B* **2006**, 110, 3330.
- (35) Spear, S. K.; Holbrey, J. D.; Rogers, R. D. *Liquid Clathrates. In Encyclopedia of Supramolecular Chemistry*; Atwood, J. L., Steed, J. W., Eds.; Marcel Dekker: New York, 2004; pp 804–808.